HHS Public Access

Author manuscript

Small. Author manuscript; available in PMC 2016 February 11.

Published in final edited form as:

Small. 2015 February 11; 11(6): 722–730. doi:10.1002/smll.201401574.

Microfluidic Gradients Reveal Enhanced Neurite Outgrowth but Impaired Guidance within 3D Matrices with High Integrin Ligand Densities

Nicole H. Romano, **Kyle J. Lampe**, **Hui Xu**, **Meghaan M. Ferreira**, and **Sarah C. Heilshorn**

476 Lomita Mall, McCullough 246, Stanford, CA 94305

Sarah C. Heilshorn: heilshorn@stanford.edu

Abstract

The density of integrin-binding ligands in an extracellular matrix (ECM) is known to regulate cell migration speed by imposing a balance of traction forces between the leading and trailing edges of the cell, but the effect of cell-adhesive ligands on neurite chemoattraction is not well understood. We present a platform that combines gradient-generating microfluidic devices with three-dimensional (3D) protein-engineered hydrogels to study the effect of RGD ligand density on neurite pathfinding from chick dorsal root ganglia-derived spheroids. Spheroids are encapsulated in elastin-like polypeptide (ELP) hydrogels presenting either 3.2 or 1.6 mM RGD ligands and exposed to a microfluidic gradient of nerve growth factor (NGF). While the higher ligand density matrix enhanced neurite initiation and persistence of neurite outgrowth, the lower ligand density matrix significantly improved neurite pathfinding and increased the frequency of growth cone turning up the NGF gradient. The apparent trade-off between neurite extension and neurite guidance is reminiscent of the well-known parabolic relationship between cell adhesion and migration speed, implying that a similar matrix-mediated balance of forces regulate neurite elongation and growth cone turning. These results have implications in the design of engineered materials for *in vitro* models of neural tissue and *in vivo* nerve guidance channels.

Keywords

neurite pathfinding; chemotaxis; elastin-like polypeptides; nerve growth factor; 3D migration

1. Introduction

Integrins are cell-surface receptors that bind specific ligands within the extracellular matrix (ECM) resulting in biochemical signaling events and the biomechanical transduction of force. Integrin ligand density is known to have a biphasic effect on cell migration over two-dimensional surfaces, whereby a minimal concentration of ligands is required to enable efficient migration, but further increasing adhesivity eventually impedes the ability of a cell to overcome traction forces at the trailing edge.[1] There is some evidence that a similar

Correspondence to: Sarah C. Heilshorn, heilshorn@stanford.edu.

Supporting Information

Supporting Information is available from the Wiley Online Library or from the author.

biphasic dependence occurs for cell migration in three-dimensional (3D) matrices, although this has been less thoroughly explored.[2–5] Of particular interest, the outgrowth of neurites, thin processes that extend from the body of a neuron, have also been reported to have a biphasic response to integrin ligand density in 3D matrices.[6] For peripheral nerve regenerative therapies, key materials selection criteria include not only the ability to stimulate neurite outgrowth, but also to guide outgrowth along a specific direction.[7–9] While many elegant designs have been reported to create materials with neurotrophic gradients to guide neurites,[10–14] the impact of integrin ligand density on neurite chemoattraction is unknown. To address this need, we present a microfluidic approach to quantitatively evaluate neurite outgrowth and guidance in response to nerve growth factor (NGF) gradients in 3D hydrogels with precise integrin ligand densities.

Biomaterials for peripheral nerve regeneration must promote neurite outgrowth through the injury gap while encouraging directional guidance toward the target of innervation.[15–17] *In vitro*, 3D neurite outgrowth has been shown to dramatically improve with the incorporation of integrin-specific cell-binding ligands in the engineered ECM.[6, 18, 19] Unlike naturally derived ECMs, synthetic matrices are capable of presenting biomimetic adhesive ligands at well-defined densities and with reproducible mechanical properties.[20–22] In particular, protein-engineered matrices fabricated from recombinant elastin-like polypeptides (ELP) enable the manipulation of integrin ligand density independent of mechanical properties such as stiffness.[23–27] The polypeptides comprising these hydrogels consist of alternating integrin-binding domains and elastin-like domains (Figure 1A). This modular design strategy enables synthesis of two recombinant ELP sequences, one with the integrin-binding RGD (Arg-Gly-Asp) sequence (termed RGD-ELP) and one with a non-active, scrambled RDG (Arg-Asp-Gly) sequence (termed ligand-free ELP). Once separately synthesized, RGD-ELP and ligand-free ELP can be mixed and covalently crosslinked to fabricate hydrogels with a desired molar concentration of integrin ligands without altering stiffness, diffusivity, or polymer weight fraction (Figure 1B).[23] We previously reported on the encapsulation of chick dorsal root ganglia (DRG) in these ELP hydrogels to demonstrate that 3D neurite outgrowth is enhanced within RGD-ELP compared to ligand-free ELP.[18]

Although the importance of adhesive ligands to neurite outgrowth has been well documented, the influence of this material parameter on neurite chemotaxis remains undefined. Local NGF gradients, in particular, play an important role in neuronal survival,[28, 29] outgrowth,[30, 31] guidance,[32, 33] and the ability of growth cones to surpass contact-inhibiting surfaces.[34] NGF gradients are widely used to stimulate neurite outgrowth and chemotaxis *in vitro* and *in vivo*, often in conjunction with naturally-derived matrices such as collagen[35, 36] and laminin,[37] amongst others.[31, 38] Immobilized gradients of NGF have also been incorporated into 3D engineered ECMs for peripheral nerve regeneration.[39, 40]

In order to study the interplay between adhesive ligand density and an NGF chemotactic gradient, we present a two-component platform: (1) a 3D ELP matrix, capable of presenting a defined density of RGD integrin ligands, within (2) a gradient-generating microfluidic device.[41] Several microfluidic devices have previously been designed to present stable gradients of neurotrophic cues to neuronal cultures.[42–45] Although microfluidic devices are

capable of presenting complex concentration profiles and multi-molecular gradients, they are often presented to cells migrating in a 2D context.[11, 13, 46] On the other hand, previous studies of 3D migration in response to soluble gradients have not benefitted from the stable and precise release profiles available within microfluidic devices.[31, 36, 43, 47–50] This system enables the quantitative evaluation of several neurite parameters, including outgrowth initiation, persistence, and growth cone turning, as a function of 3D integrin ligand density within a stable NGF gradient. Interestingly, we find that the higher ligand density matrix enhances neurite outgrowth and persistence, while the lower ligand density matrix results in improved neurite guidance toward the NGF source. This implies that the choice of matrix for peripheral nerve regeneration may require a trade-off between the rate of neurite outgrowth and the chemotaxis-driven directionality toward an innervation target. Furthermore, this two-component microfluidic platform may be broadly useful in the evaluation of matrix parameters that mediate 3D chemotaxis.

2. Results and Discussion

2.1. Stable NGF gradient formation through ELP hydrogels

The gradient-generating microfluidic devices were fabricated from PDMS using soft lithography techniques (Figure 2A). By initiating flow through the source and sink channels before injecting a hydrogel precursor solution into the central cell culture chamber, the hydrogel could be reproducibly cast without leakage into the capillaries or flanking source and sink channels. Furthermore, because the capillaries feature a small cross-section (10 μm × 15 μm) in comparison to the chamber (4 mm × 160 μm), gradients are established by diffusion of solute molecules through the capillaries without inducing the convective flow and shear stress known to cause growth cone collapse.[51] Using 10 kDa Texas Red-conjugated dextran as a fluorescent probe, we confirmed that a precise gradient forms within 2 hours and remains stable over the course of at least 8 hours (Figure 2A). The gradient spans a range of 47% to 25% of the source concentration across the 1-mm width of the central chamber (linear regression of 10 gradients over 8 hours, $R^2 = 0.96$), corresponding to a gradient slope of 11.5 ng mL^{-1} mm^{-1} of NGF with a range of 12.5 ng mL^{-1} to 23.5 ng mL^{-1} NGF, a concentration range previously demonstrated to induce DRG neurite outgrowth.[52]

2.2. Neurite outgrowth within 3D ELP matrices in microfluidic devices

Previous studies evaluated the outgrowth of neurites from DRGs encapsulated in 3D ELP matrices with elastic moduli ranging from 0.5 kPa to 2.0 kPa.[18] Outgrowth was enhanced in the most compliant ELP matrix formulation, corresponding to a 3 wt% ELP hydrogel with 1.32 mM THPC crosslinker. Therefore, we selected an identical protein polymer concentration and crosslinking density to fabricate our 3.2 mM and 1.6 mM RGD-ELP matrices, which corresponds to about 2 and 1×10^6 RGD ligands μm^{-3}, respectively.

Immunocytochemistry of growing spheroids within the microfluidic devices revealed elongating neurites with co-migrating Schwann cells (Figure 2B–E). Although explant cultures often present a varied cell population, co-localization of Hoechst stain for nuclei with either the neuronal marker β-III tubulin or the Schwann cell marker S-100 protein

confirmed the absence of any major contaminating cell types. In all cultures, Schwann cells were predominantly observed to be in contact with the outgrowing neurites, consistent with Schwann cell-neurite behavior in the weeks leading to axon myelination.[53, 54] This immunocytochemistry confirms that DRG-derived co-cultures remain viable for at least 2 days when encapsulated in ELP matrices within a microfluidic device.

2.3. Initiation is more directed in 1.6 mM RGD-ELP

Based on qualitative evaluation, spheroids encapsulated in 3.2 mM RGD-ELP demonstrated enhanced overall outgrowth as compared to spheroids encapsulated in the less adhesive matrix (Figure 3A, B). As a first measure of the effect of the NGF gradient on neurite outgrowth, we compared the number of neurites initiated on the source-facing spheroid edge to those initiated on the opposite, sink-facing spheroid edge. Neurites crossing the 10 μm benchmarks in either direction were defined as initiated (Figure 3C). For both RGD concentrations of ELP hydrogels, the incidence of neurite initiation toward the NGF source was more frequent than that of neurites initiating away from the NGF source ($p < 0.05$, n = 44 spheroids in 5 devices for 3.2 mM RGD-ELP, n = 63 spheroids in 7 devices for 1.6 mM RGD-ELP, Figure 3D). Although the average number of neurites initiated per spheroid in the 1.6 mM RGD-ELP was decreased by 76% compared to the average number of neurites initiated per spheroid in the 3.2 mM RGD-ELP matrix, the ratio of neurites initiated toward the NGF source versus away was significantly enhanced in the less adhesive matrix ($p < 0.0001$, two-proportion z-test).

After initiation, interaction with an engineered ECM microenvironment can stimulate a variety of behaviors in outgrowing neurites. Some possible responses include branching to maximize neuron-matrix interactions, turning in response to chemotactic cues, and modulating migratory speed. Similar to initiation bias, the outgrowth ratio compares the number of neurites growing up or down the NGF gradient as they extend out to 200 μm into the RGD-ELP matrix. For symmetric neurite outgrowth, *i.e.* no bias toward the NGF source, the outgrowth ratio is defined to be 1. Neurite outgrowth toward the chemoattractive target increases the outgrowth ratio index, while similar outgrowth in the opposite direction drives the index closer to 1.

Outgrowth ratio in 3.2 mM RGD-ELP indicated a directional bias toward increasing NGF concentration at all distances tested ($p < 0.005$ for each of 10, 50, 100, 150 and 200 μm from the spheroid edge, z-test with $H_0 = 1$). In comparison, the outgrowth ratios in the 1.6 mM RGD-ELP matrix were improved by almost two-fold over the 3.2 mM RGD-ELP matrix ($p < 0.0001$, two-proportion z-test, Figure 3E). Although previous studies of PC12 cells in agarose hydrogels suggest that an NGF gradient of at least 133 ng mL^{-1} mm^{-1} is required for neurite guidance,[10] the 11.5 ng mL^{-1} mm^{-1} gradient was sufficient to generate biased outgrowth from DRG neurons within our RGD-ELP hydrogels. In both matrices, the biased outgrowth ratio improved over longer distances, indicating that neurites growing toward the NGF source extend farther through the RGD-ELP matrix, compared to those extending toward the sink. This enhanced bias at longer distances could be due to 1) increased neurite persistence toward the NGF source and/or 2) increased turning of neurites initiated toward

the sink. To evaluate these two possibilities (which are not mutually exclusive), we tracked individual neurite paths for their persistence and turning events.

2.4. Persistence is enhanced in 3.2 mM RGD-ELP

Although the lower integrin-binding ligand density matrix enhanced outgrowth ratio, neurites in 3.2 mM RGD-ELP were capable of persisting farther through the matrix. In order to quantify this observation, we measured the likelihood of neurites to extend to a particular distance without significantly changing course. While outgrowth ratio measures all neurite events regardless of their individual neurite paths (for example, branching or turning events), the persistence metric requires tracking of each individual initiated neurite.

Neurite persistence toward the NGF source was significantly greater in the 3.2 mM RGD-ELP matrix than in the 1.6 mM RGD-ELP matrix ($p < 0.01$ for 100, 150 and 200 μm, Figure 4A). While this trend was also observed for neurites extending down the gradient, the effect was not significant (Figure 4B). Within the more adhesive matrix, neurites initiated toward the NGF source were significantly more likely to persist to 100, 150 and 200 μm than those initiated away ($p < 0.05$ for 100, 150 and 200 μm, Wilcoxon test, Figure S1), while no significant difference in persistence toward or away from the NGF source was observed in the less adhesive matrix. Therefore, while initiation of the neuritic processes exhibited enhanced sensitivity to the NGF gradient in the 1.6 mM RGD-ELP matrix, the ability to persist due to the NGF gradient was only enhanced in the 3.2 mM RGD-ELP matrix.

2.5. Turns are more frequent and reflect fine-tuning of pathfinding in 1.6 mM RGD-ELP

Next, to quantify the ability of neurites to turn toward the NGF source, we evaluated the individual paths of all neurites, regardless of their initiation site on the spheroid (Figure 4C). All turning events greater than 30° and persisting at the new angle for at least 50 μm were evaluated for turn size and direction. While 43% of all neurites exhibited at least one turn in the 1.6 mM RGD-ELP matrix, only 15% of neurites made qualifying turns in the 3.2 mM RGD-ELP matrix (Figure 4D). Of the neurite turns in the 3.2 mM RGD-ELP matrix, no significant overall bias in turn direction was found (43 of 72 turns were toward the source, $p = 0.08$, one-proportion z-test with $H_0 = 0.5$). In contrast, turns in the 1.6 mM RGD-ELP matrix were two-fold more likely to turn toward the NGF source than away (30 of 44 turns were toward the source, $p < 0.0001$, one-proportion z-test rejecting $H_0 = 0.5$).

We then performed a contingency analysis to explore whether the neurite orientation before a turn (θ_i) influenced the likelihood to turn toward or away from the NGF source (Figure 5A). Neurites that were oriented away from the NGF source prior to turning were highly likely to turn toward the NGF source ($p < 0.0001$ for both materials, contingency analysis and one-proportion z-test with $H_0 = 0.5$, Figure 5A, Table S1), regardless of the integrin-binding ligand density of the matrix. The incidence of ‘mis-guidance’ (*i.e.* a turn away from the NGF source) was more frequently observed in neurites oriented toward the NGF source (as opposed to away from the NGF source) before turning (Figure 5A). It should be noted that, because only turns greater than 30° were counted, neurites initially oriented within 30° of the meridian could not make a turn toward the source great enough to be counted. Nevertheless, these ‘mis-guidance’ events were more likely to occur in the 3.2 mM RGD-

ELP matrix than in the matrix presenting a lower integrin-binding ligand density ($p < 0.005$, z-test of two proportions, Figure 5A).

We then evaluated the size of these turns (θ_{turn}) as a function of turn direction and integrin-binding ligand density. Turning events toward the NGF source in the 3.2 mM RGD-ELP matrix were significantly larger in size than those directed away from the source in the same matrix or in either direction within the 1.6 mM RGD-ELP matrix ($p < 0.005$, t-tests, Figure 5B). The nuanced turning behavior in these two matrices is best understood by visualizing an overlay of all turning neurites (Figure 5C, D). In the 3.2 mM RGD-ELP matrix, overall neurite guidance is largely achieved through persistence of neurites initially oriented toward the source and dramatic turns up the gradient for neurites initially oriented away (Figure4A and 5C). In contrast, guidance in the less adhesive matrix primarily relies on the highly biased initiation of neurites toward the source and subsequent fine-tuning of outgrowth direction (Figure3D and 5D).

Our results suggest that the reduction of RGD ligand density from 3.2 mM to 1.6 mM has adjusted the balance of cell-matrix interactions in favor of growth cone guidance to the detriment of outgrowth distance. These results underscore the potential impact of integrin-binding ligand density in promoting efficient, targeted neurite outgrowth within neurotrophic gradients. Furthermore, these data suggest that the design of engineered matrices for peripheral nerve guidance channels may benefit from the conscientious presentation of integrin-binding ligands at a density that balances neurite outgrowth with pathfinding ability.

3. Conclusion

We have combined a gradient-generating microfluidic device with 3D protein-engineered hydrogels to study the role of integrin-binding ligand density on neurite outgrowth and pathfinding in response to an NGF gradient. While earlier reports have demonstrated the importance of RGD ligand density in mediating neurite outgrowth, its role in enabling 3D neurite pathfinding was previously unknown. We show that neurite initiation frequency and persistence are significantly enhanced within engineered RGD-ELP hydrogels presenting 3.2 mM RGD ligands, as compared to similar hydrogels presenting 1.6 mM RGD ligands. In contrast, neurites in 1.6 mM RGD-ELP matrices are more sensitive to the NGF gradient, resulting in greater initiation, enhanced outgrowth bias, and increased frequency of growth cone turning toward the NGF source. Therefore, directed outgrowth patterns were a result of increased persistence in the 3.2 mM RGD-ELP matrix and increased likelihood of turning in the 1.6 mM RGD-ELP matrix. Taken together, these data imply a potential trade-off between neurite outgrowth and guidance toward a chemoattractive target that can be tuned with integrin-binding ligand density in 3D engineered matrices. These results will prove useful in the design and selection of engineered materials for peripheral nerve regeneration. Additionally, this experimental platform, which combines a microfluidic gradient-generating device with an engineered 3D ECM, should be broadly useful in the evaluation of matrix parameters that mediate 3D chemotaxis for a range of biological systems.

4. Materials and Methods

ELP production, purification, and gelation

Elastin-like polypeptides (ELPs) were fabricated using protein-engineering techniques and temperature cycling purification, as previously described.[55] A plasmid encoding the recombinant ELP was transformed into BL21(DE3) *Escherichia coli* and cloned for sequence uniformity. A colony of *E. coli* was fermented in 12-L batches of Terrific Broth (Life Technologies, Carlsbad, CA) supplemented with 4 g L^{-1} glycerol. After reaching an OD_{600} of 0.8, target protein translation was induced by the addition of 1 mM isopropyl β-D-1-thiogalactopyranoside (IPTG, Sigma, St. Louis, MO). Protein production was allowed to proceed for four to six hours before the bacteria were pelleted. The wet cell pellet was lysed by sonication in TEN buffer (0.01 M Tris, 0.001 M EDTA, 0.1 M NaCl, pH 8.0) in the presence of 1 mM phenylmethylsulfonyl fluoride protease inhibitor (PMSF, Sigma). ELP was purified from cell debris by repeated temperature cycling between 4°C and 37°C accompanied by centrifugation. During 4°C cycles, the pH was adjusted to 9.0 to improve solubility of ELP, while 1 M NaCl assisted with ELP precipitation during 37°C cycles. The purified protein was dialyzed against water with a 10 kDa MWCO membrane to remove excess salts, and the product was stored in a lyophilized state. ELP purity was confirmed by SDS-PAGE.

ELP hydrogels were crosslinked using tetrafunctional tetrakis(hydroxymethyl)phosphonium chloride (THPC) crosslinker (Sigma). All ELP and crosslinker solutions were separately sterilized using 0.22 μm filters prior to mixing. For 3.2 mM RGD-ELP hydrogels, all ELP contained the integrin-binding RGD domain, while 1.6 mM RGD-ELP was achieved by mixing RGD-ELP with ligand-free ELP in a 1:1 ratio before crosslinking. Hydrogel precursor solutions prepared in phosphate buffered saline (PBS) were comprised of 3 wt% ELP with 1.32 mg ml^{-1} THPC, corresponding to a final ratio of 1:2 hydroxymethyl groups to primary amines on the peptide backbone.

Microfluidic device fabrication

Microfluidic gradient generating devices (Figure 2A) were designed in AutoCAD (AutoDesk, San Rafael, CA) and fabricated using common soft lithography techniques, as previously reported.[41] The master mold consisted of two layers of SU-8 photoresist, a 10-μm capillary layer and a 160-μm chamber layer, respectively, on a Si wafer (Stanford Microfluidic Foundry, Stanford, CA). Before fabricating polydimethylsiloxane (PDMS) devices from this mold, the wafer was treated with (3-aminopropyl) trimethoxysilane (Sigma, St. Louis, MO) overnight. Sylgard 184 monomer and crosslinker (Dow Corning, Corning, NY) were thoroughly mixed in a 10:1 ratio, degassed for 20 minutes, and poured over the master mold. After 1 hour at 65°C, the resulting PDMS layer was separated from the master mold and cut into individual devices. A tissue biopsy punch (0.042 inch outer diameter, SYNEO Corporation, Angleton, TX) was used to punch inlet and outlet ports for the central chamber, source channel, and sink channel. Finally, the devices were irreversibly bonded in 2-well glass bottom culture chambers (Mat-Tek) by plasma-treating contact surfaces for 30 seconds and incubating at 60°C for 30 minutes. During experiments, a constant flow of nutrients was provided by a push-pull syringe pump assembled with 250-μL

gastight glass syringes, PTFE Luer Lock hubs and 26-gauge PTFE tubing (all from Hamilton, Reno, NV).

Spheroid preparation

Dorsal root ganglia (DRGs) were isolated from embryonic chicks at day 9 (E9) and suspended in NGF-supplemented DRG medium: Dulbecco's modified Eagle medium plus 10 % fetal bovine serum, 1 % penicillin-streptomycin (Sigma), and 50 ng ml^{-1} nerve growth factor (Life Technologies). Immediately following isolation, 60 DRGs were dissociated in warm collagenase (200 U mL^{-1}, Sigma) and incubated at 37°C for 10 minutes. After triturating to break up the structures, 10× trypsin inhibitor (Invitrogen) was added to halt collagenase activity. The cell suspension was pelleted, resuspended in DRG medium with NGF, and centrifuged in a single well of an AggreWell 400 plate (StemCell Technologies, Vancouver, BC) according to manufacturer protocol. After 24 hours of incubation, the spheroids were ready for encapsulation.

Device loading and culture

Devices were rinsed three times each with ethanol and PBS before being submerged in DRG medium without NGF supplementation. Before loading the central chamber with ELP hydrogel precursor, the source inlet was connected to a syringe containing DRG medium supplemented with 50 ng mL^{-1} NGF, and the sink inlet was connected to a syringe containing non-supplemented DRG medium. A continuous flow rate of 2.5 μL hr^{-1} was maintained in both the source and sink channels during loading of the ELP gel precursor and throughout the rest of the experiment. To load the central chamber, a precursor RGD-ELP gel solution (5 μL) without spheroids was pipetted by hand into the central chamber inlet, followed by a precursor RGD-ELP gel solution (5 μL) containing spheroids. The devices were allowed to remain at room temperature for 12 minutes, to ensure gelation, before transferring the entire setup to an incubator. Spheroid outgrowth was allowed to proceed for 2 days in the gradient generating device (2.5 μL hr^{-1} flow rate) at 37 °C, 5% CO_2 and 100% humidity before data acquistion.

Microfluidic device characterization

Visualization of the gradient was performed using 10 kDa Texas Red-conjugated dextran (Invitrogen) as an analog for NGF, which has a molecular weight of 13.2 kDa. The source contained 3 μM dextran in phenol red-free DMEM, while the sink supplied phenol red-free DMEM alone. An ELP hydrogel without spheroids was prepared in the device as described above, and dextran fluorescence was monitored across the central chamber at 10× magnification with an inverted fluorescent microscope (Zeiss, Axiovert 200M) over the course of eight hours, with image acquisition occurring every 15 minutes.

Staining and visualization of spheroids

Spheroid outgrowth was visualized by staining metabolically active cells with 6 μM calcein acetomethylester and dead cells with 2 μM ethidium homodimer-1 (Live/Dead kit, Life Technologies). After 2 days of culture, devices were rinsed by flowing phenol red-free DMEM through the source and sink channels for 10 minutes, followed by flowing the Live/

Dead solution through the source and sink channels for 40 minutes of staining, all at a rate of 10 μL hr^{-1} at 37 °C with 5% CO_2 and 100% humidity.

For immunocytochemistry, the cultures were fixed by hand-injecting 4% paraformaldehyde into the source and sink channels prior to a static overnight incubation at 37°C. All subsequent steps were performed at 4°C under a continuous flow rate of 10 μL hr^{-1}, with one syringe connected to the source inlet and a second syringe connected to the source outlet. The central chamber ports were plugged to induce perfusion across the central chamber and into the sink channel. Then, the devices were rinsed with PBS plus 0.4% sodium azide for 3 hours and permeabilized with PBS plus 0.25 % Triton X-100 for 1 hour. The devices were again rinsed in PBS for 1 hour and blocked for 4 hours in PBS with 5% bovine serum albumin (BSA), 5% fetal goat serum, and 0.5% Triton X-100. The primary antibody solution, consisting of rabbit anti-S100 at a 1:200 dilution (Sigma) and mouse anti-β-III tubulin at a 1:250 dilution (Promega, Madison, WI) in PBS with 2.5% BSA and 0.25% Triton X-100, was applied overnight under continuous flow. The device was rinsed with PBS plus 0.4% sodium azide for 8 hours, followed by a secondary antibody solution containing goat anti-mouse AlexaFluor 555 and goat anti-rabbit AlexaFluor 488 (1:250 each, Life Technologies) overnight. Finally, the devices were rinsed for 4 hours in PBS before imaging.

Three-dimensional outgrowth of spheroids was visualized on a Leica SPE confocal microscope. Each device was imaged completely at either 10× or 20× magnification by automatic xy tiling of >100 μm z-stacks (2.4 μm step size) in Leica's LAS AF software. Z-stacks were compressed into maximum projections for outgrowth quantification.

Analysis Methods: Initiation

Only spheroids at least 200 μm from the source and sink channels were used in data collection to allow sufficient distance from the channel walls for neurite outgrowth. To assess the number of neuritic processes that were initiated toward the source and sink, lines perpendicular to the gradient (with a length equal to the spheroid diameter) were drawn at 10 μm, 50 μm, 100 μm, 150 μm and 200 μm distances from the edge of the spheroid, toward both the source and the sink (Figure 3C). In ImageJ, profile plots revealed the number of neurite outgrowths that intersected each of these lines, and this digital analysis was visually confirmed for each individual outgrowth to correct for false digital counts due to migrating Schwann cells. The number of initiated neurites per spheroid was defined as the number of neurites intersecting the 10 μm benchmarks in each direction.

The outgrowth ratio metric was adapted from Rosoff, *et al*.[36] At each distance, the outgrowth ratio was defined by Equation 1, where n_i is the number of neurites passing a given benchmark from spheroid *i*. This results in an outgrowth ratio of 1 for symmetric outgrowth and a bias greater than 1 for directional outgrowth toward the NGF source.

$$i=1snisourceini\ \text{sink}. \quad (1)$$

Analysis Methods: Persistence

The percent persistence measures the likelihood of individual neurites to persist through the RGD-ELP matrix in a particular direction. Each initiated neurite (as defined above) was manually tracked to evaluate whether it traversed the 50 μm, 100 μm, 150 μm and 200 μm benchmarks. For each spheroid, the percent persistence at a given distance was defined as the percent of neurites crossing each benchmark relative to the number of initiated neurites. At each distance from the spheroid edge, source and sink persistence percentages were compared using the Wilcoxon test for non-parametric, paired data.

Analysis Methods: Turning

All neurite turns greater than 30° were catalogued for turn size and direction, provided that the neurite persisted for at least 50 μm at the new angle. The neurite's initial and final orientation ($\theta_{initial}$ and θ_{final}, respectively) were determined relative to the meridian (Figure 4C). Neurites oriented between 0° and 90° before turning were considered to be oriented toward the NGF source, while those oriented between 90° and 180° were considered to be oriented away. Turn size was defined as $\theta_{initial} - \theta_{final}$, where a positive turn angle indicated a turn toward the NGF source. Although multiple turns in a single neurite were rare, all qualifying turns were included in the analysis.

In addition to the orientation and turn angles, the entire paths of turning neurites were tracked using the Manual Tracking plugin in ImageJ. The tracks were exported as comma-separated value (.csv) files, transformed from pixel coordinates to a Cartesian coordinate system, and scaled to reflect distance in microns. The tracks were visualized in R (R Foundation for Statistical Computing, Vienna, Austria) using the ggplot2 package.[56]

Statistics

Neurite outgrowth into ligand-containing ELP gels was evaluated in 5 devices for 3.2 mM RGD-ELP (n = 44 spheroids) and 7 devices for 1.6 mM RGD-ELP (n = 63 spheroids), each over the course of multiple experiments. Statistical tests were performed in Prism (GraphPad, La Jolla, CA) and R. Comparison of ratios, such as the initiation bias or outgrowth ratio as a result of integrin ligand density, was performed using a two-proportion z-test. For quantification of turning behavior, 478 neurites were tracked in 3.2 mM RGD-ELP matrices and 99 neurites were tracked in 1.6 mM RGD-ELP. To evaluate the significance of turning frequency in a particular direction, the proportion of turns in that direction was compared to $H_0 = 0.5$, *i.e.* no bias in turn direction, using a one-proportion z-test (n = 72 turning neurites in 3.2 mM RGD-ELP and n = 44 turning neurites in 1.6 mM RGD-ELP). For the purposes of visualizing turn bias in the context of all tracked neurites (Figure 4D), the percent of all neurites turning toward the NGF source was compared to the percent turning away using a two-proportion z-test (n = 478 neurites tracked in 3.2 mM RGD-ELP, n = 99 neurites tracked in 1.6 mM RGD-ELP).

Supplementary Material

Refer to Web version on PubMed Central for supplementary material.

Acknowledgements

N.H.R. acknowledges support from a Stanford Graduate Fellowship and a National Science Foundation Graduate Fellowship. K.J.L acknowledges support from NIH NRSA F32NS076222. M.M.F. acknowledges support from a National Science Foundation Graduate Fellowship and the Stanford Diversifying Academia, Recruiting Excellence Fellowship. The authors acknowledge funding from the National Institutes of Health (1DP2-OD006477, R01-DK085720, R21-AR062359-01) and the National Science Foundation (DMR-0846363). The authors thank Ruby E. Dewi (Stanford University) for help with gradient quantification, as well as Amy Proctor (Stanford University) for assistance with ELP hydrogels.

References

1. Palacek SP, Loftus JC, Ginsberg MH, Lauffenburger DA, Horwitz AF. Nature. 1997; 385(6616): 537–540. [PubMed: 9020360]
2. Hoffmann J, West J. Integrative Biology. 2013; 5(5):817–827. [PubMed: 23460015]
3. Zaman MH, Kamm RD, Matsudaira P, Lauffenburger DA. Biophysical Journal. 2005; 89(2):1389–1397. [PubMed: 15908579]
4. Zaman MH, Trapani LM, Siemeski A, MacKellar D, Gong H, Kamm RD, Wells A, Lauffenburger DA, Matsudaira P. Proceedings of the National Academy of Sciences. 2006; 103(37):13897–13897.
5. Doyle AD, Petrie RJ, Kutys ML, Yamada KM. Current Opinion in Cell Biology. 2013; 25(5):642–649. [PubMed: 23850350]
6. Schense JC, Hubbell J. Journal of Biological Chemistry. 2000; 275(10):6813–6818. [PubMed: 10702239]
7. Jiang X, Lim SH, Mao H-Q, Chew SY. Experimental Neurology. 2010; 223(1):86–101. [PubMed: 19769967]
8. Belkas JS, Shoichet MS, Midha R. Operative Techniques in Orthopaedics. 2004; 14(3):190–198.
9. Bellamkonda RV. Biomaterials. 2006; 27(19):3515–3518. [PubMed: 16533522]
10. Cao X, Shoichet MS. Neuroscience. 2001; 103(3):831–840. [PubMed: 11274797]
11. Joddar B, Guy A, Kamiguchi H, Ito Y. Biomaterials. 2013; 34(37):9593–9601. [PubMed: 24021758]
12. Kapur TA, Shoichet MS. Journal of Biomedical Materials Research Part A. 2004; 68(2):2335–2343.
13. Li G, Liu J, Hoffman-Kim D. Annals of Biomedical Engineering. 2008; 36(6):889–904. [PubMed: 18392680]
14. Tang S, Zhu J, Xu Y, Xiang AP, Jiang MH, Quan D. Biomaterials. 2013; 34(29):7086–7096. [PubMed: 23791502]
15. Nisbet, Crompton KE, Horne MK. Journal of Biomedical Materials Research B. Applied Biomaterials. 2008; 87(1):251–263. [PubMed: 18161806]
16. Scheib J, Hoke A. Nature Reviews Neurology. 2013; 9(12):668–676. [PubMed: 24217518]
17. Yiu G, He Z. Nature reviews. Neuroscience. 2006; 7(8):617–627. [PubMed: 16858390]
18. Lampe K, Antaris A, Heilshorn S. Acta Biomaterialia. 2013; 9(3):5590–5599. [PubMed: 23128159]
19. Shepard JA, Stevans AC, Holland S, Wang CE, Shikanov A, Shea LD. Biotechnology and bioengineering. 2012; 109(3):830–839. [PubMed: 22038654]
20. DiMarco RL, Heilshorn SC. Advanced Materials. 2012; 24(29):3923–3940. [PubMed: 22730248]
21. Lutolf MP, Hubbell JA. Nat Biotech. 2005; 23(1):47–55.
22. Hyun J, Ma H, Banerjee P, Cole J, Gonsalves K, Chilkoti A. Langmuir. 2002; 18(8):2975–2979.
23. Chung C, Lampe K, Heilshorn S. Biomacromolecules. 2012; 13(12):3912–3916. [PubMed: 23151175]
24. Straley KS, Heilshorn SC. Front. Neuroeng. 2009; 2(9):1–10. [PubMed: 19194527]
25. Gagner JE, Kim W, Chaikof EL. Acta Biomaterialia. 2014; 10(4):1542–1557. [PubMed: 24121196]
26. Di Zio K, Tirrell DA. Macromolecules. 2003; 36(5):1553–1558.

27. Simnick AJ, Lim DW, Chow D, Chilkoti A. Polymer Reviews. 2007; 47(1):121–154.
28. Herrup K, Shooter EM. Proceedings of the National Academy of Sciences. 1973; 70(12):3884–3888.
29. Kaplan, Hempstead BL, Martin-Zanca D, Chao MV. Science. 1991; 252(5005):554–558. [PubMed: 1850549]
30. Hari A, Djohar B, Skutella T, Montazeri S. International Journal of Developmental Neuroscience. 2004; 22(2):113–117. [PubMed: 15036386]
31. Letourneau P. Developmental Biology. 1978; 66(1):183–196. [PubMed: 751835]
32. Gallo G, Lefcort F, Letourneau P. The Journal of Neuroscience. 1997; 17(14):5445–5454. [PubMed: 9204927]
33. Gundersen R, Barrett JN. The Journal of Cell Biology. 1980; 87(3):546–554. [PubMed: 6257725]
34. Kaselis A, Treinys R, Vosyliute R, Satkauskas S. Cellular and Molecular Neurobiology. 2014; 34(2):289–296. [PubMed: 24338202]
35. Mortimer D, Pujic Z, Vaughan T, Thompson A, Feldner J, Vetter I, Goodhill G. Proceedings of the National Academy of Sciences. 2010; 107(11):5202–5207.
36. Rosoff W, Urbach J, Esrick M, McAllister R, Richards L, Goodhill G. Nature Neuroscience. 2004; 7(6):678–682. [PubMed: 15162167]
37. Yu X, Dillon G, Bellamkonda R. Tissue Engineering. 1999; 5(4):291–304. [PubMed: 10477852]
38. Li G, Hoffman-Kim D. Tissue Engineering Part B. Reviews. 2008; 14(1):33–51. [PubMed: 18454633]
39. Dodla M, Bellamkonda R. Biomaterials. 2008; 29(1):33–46. [PubMed: 17931702]
40. Yu L, Miller F, Shoichet M. Biomaterials. 2010; 31(27):6987–6999. [PubMed: 20579725]
41. Shamloo A, Heilshorn SC. Lab on a Chip. 2010; 10(22):3061–3068. [PubMed: 20820484]
42. Dupin I, Dahan M, Studer V. Journal of Neuroscience. 2013; 33(45):17647–17655. [PubMed: 24198357]
43. Sip C, Bhattacharjee N, Folch A. Lab on a Chip. 2014; 14(2):302–314. [PubMed: 24225908]
44. Bhattacharjee N, Li N, Keenan T, Folch A. Integrative Biology. 2010; 2(11–12):669. [PubMed: 20957287]
45. Kothapalli CR, van Veen E, de Valence S, Chung S, Zervantonakis IK, Gertler FB, Kamm RD. Lab on a Chip. 2011; 11(3):497–507. [PubMed: 21107471]
46. Wang CJ, Li X, Lin B, Shim S, Ming G, Levchenko A. Lab on a Chip. 2008; 8(2):227–237. [PubMed: 18231660]
47. Tehranirokh M, Kouzani AZ, Francis PS. Microsystem. 2013; 19(4):623–628.
48. Lühmann T, Hall H. Materials. 2009; 2(3):1058–1083.
49. Cao X, Shoichet MS. Neuroscience. 2003; 122(2):381–389. [PubMed: 14614904]
50. Pujic Z, Goodhill GJ. Journal of Neuroscience Methods. 2013; 215(1):53–59. [PubMed: 23453927]
51. Wang CJ, Li X, Lin B, Shim S, Ming GL, Levchenko A. Lab on a Chip. 2008; 8(2):227–237. [PubMed: 18231660]
52. Mortimer D, Feldner J, Vaughan T, Vetter I, Pujic Z, Rosoff WJ, Burrage K, Dayan P, Richards LJ, Goodhill GJ. Proceedings of the National Academy of Sciences. 2009; 106(25):10296–10301.
53. Webster HD, Martin JR, O'Connell MF. Developmental Biology. 1973; 32(2):401–416. [PubMed: 4789698]
54. Wanner IB, Wood PM. Journal of Neuroscience. 2002; 22(10):4066–4079. [PubMed: 12019326]
55. Straley KS, Heilshorn SC. Soft Matter. 2009; 5(1):114.
56. Wickham, H. ggplot2: elegant graphics for data analysis. New York: Springer; 2009.

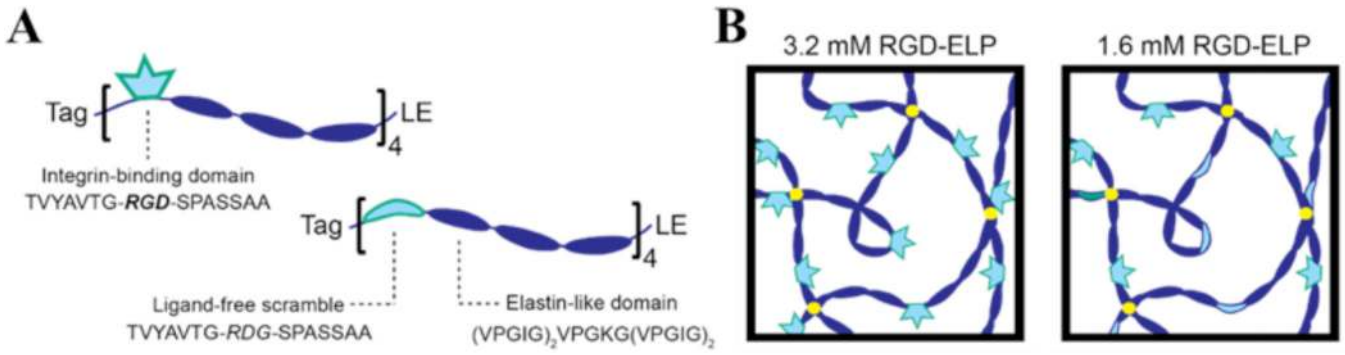

Figure 1.

Schematic of RGD-ELP hydrogels with tunable control of integrin-binding ligand density. **A,** RGD-ELP contains the bioactive RGD ligand, while ligand-free ELP contains a non-active scrambled sequence. **B,** Schematic of a 3.2 mM RGD-ELP hydrogel, composed entirely of protein containing the bioactive RGD ligand, and **C,** 1.6 mM RGD-ELP, composed of a 1:1 ratio of RGD-ELP and ligand-free ELP, with identical hydrogel density and stiffness.

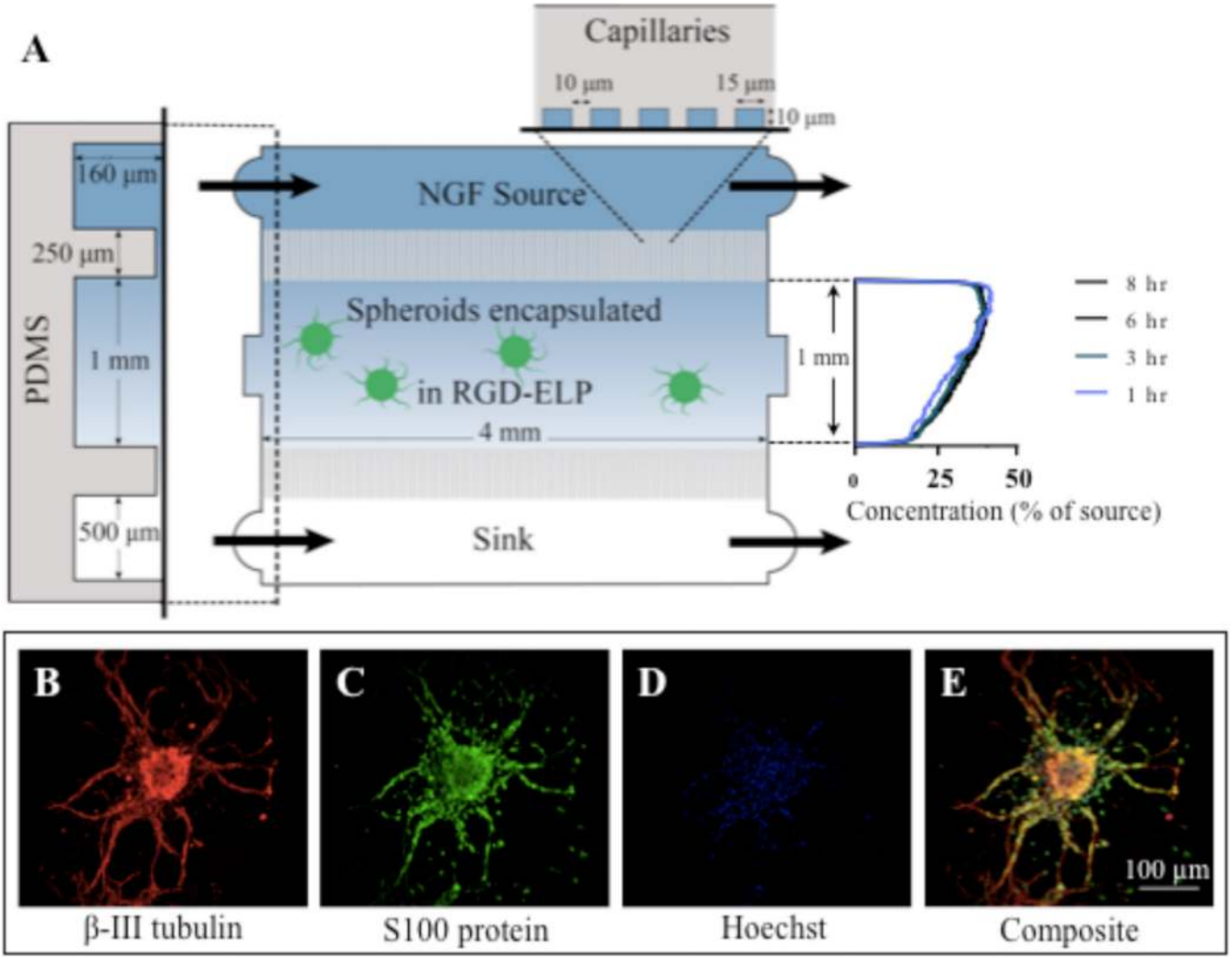

Figure 2.

Microfluidic generation of NGF gradient through a 3D ELP hydrogel. **A**, Design and dimensions of the PDMS device. The gradient is stable through an ELP hydrogel over the course of at least 8 hours. **B–E,** Neural spheroid outgrowth after 2 days of encapsulation in 3.2 mM RGD-ELP within the device. NGF source is oriented at the top of the images. Spheroids were stained for beta-III tubulin (neuronal marker) (**B**), S100 protein (Schwann cell marker) (**C**), and Hoechst (nuclei) (**D**). The overlay **E** shows the interaction between Schwann cells (green) and outgrowing neurites (red).

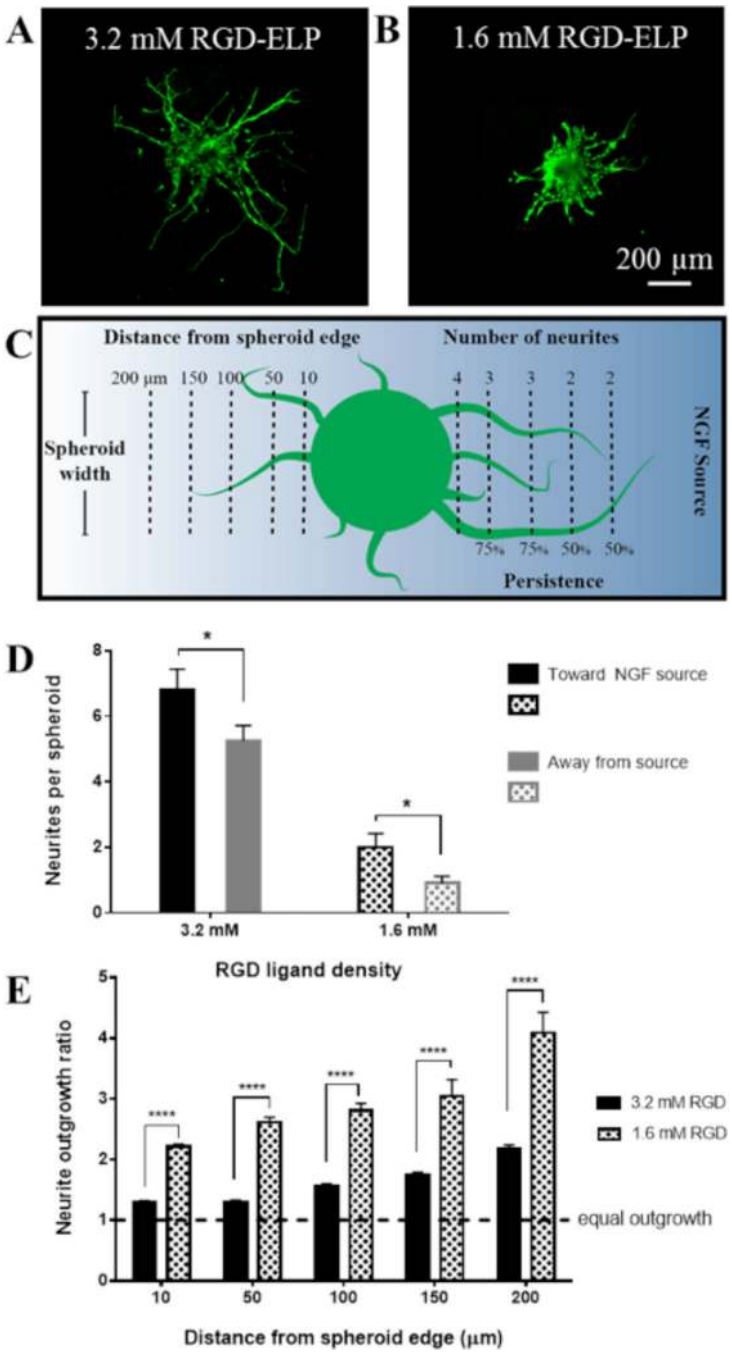

Figure 3.

A, B Representative spheroids stained with Live/Dead in 3.2 mM **(A)** and 1.6 mM **(B)** RGD-ELP after two days of culture. **C,** Schematic of analysis for initiation, outgrowth ratio and persistence. **D,** Initiation of neurites from encapsulated spheroids toward or away from the NGF source. **E,** Outgrowth ratio, defined as the ratio of neurites extending toward or away from the NGF source at a given distance from the spheroid edge. * $p < 0.05$, **** $p < 0.0001$. All graphs show mean ± SEM.

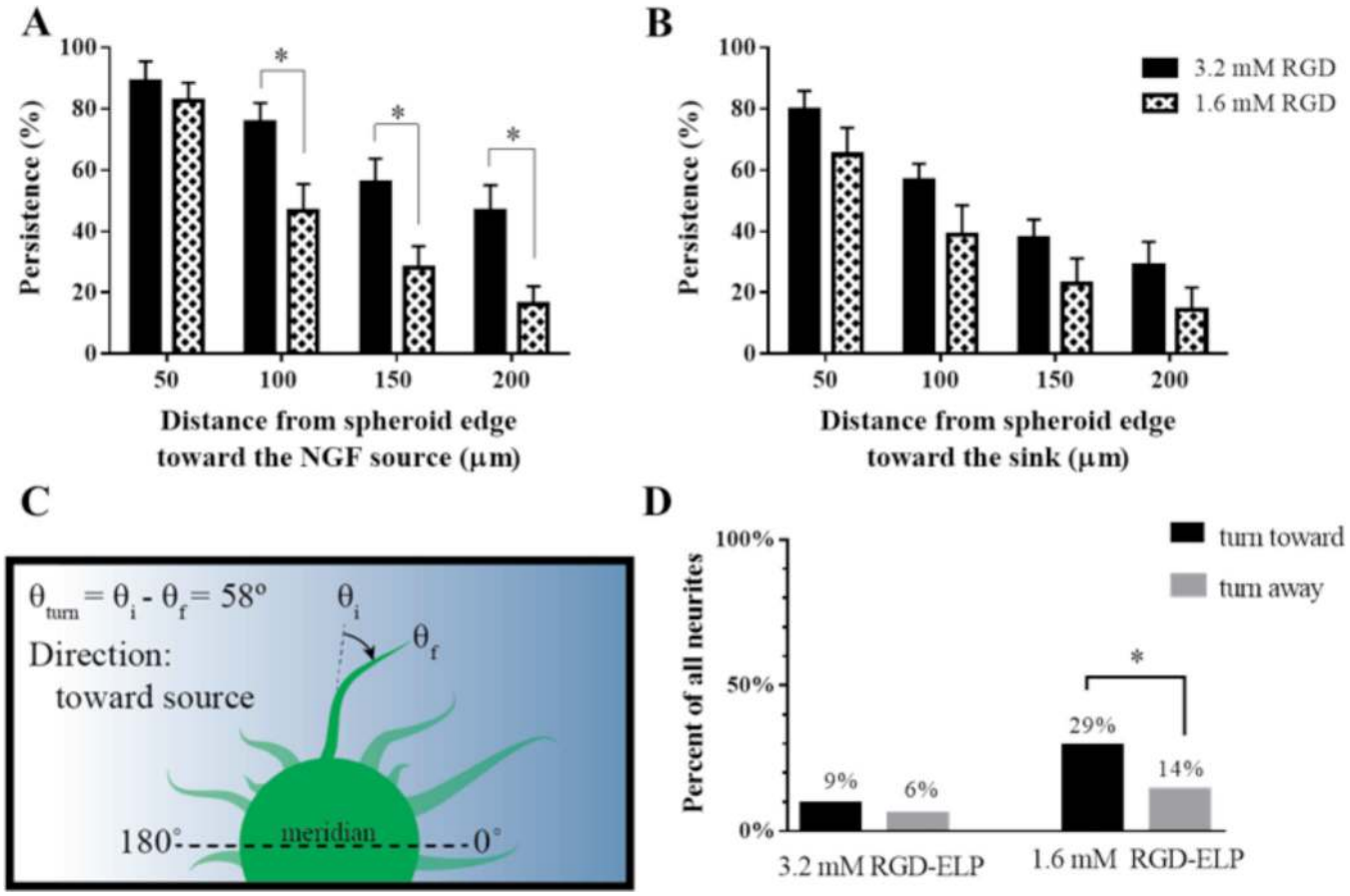

Figure 4.

Persistence of neurites through the RGD-ELP hydrogel. **A**, Neurites elongating toward the NGF source are more likely to persist through 3.2 mM RGD-ELP as compared to 1.6 mM RGD-ELP. **B,** Neurites extending away from the source do not exhibit statistically enhanced persistence as a function of RGD ligand density. Graphs depict mean ± SEM. **C,** Schematic of turning measurements. **D,** Frequency of neurite turning in 3.2 mM and 1.6 mM RGD-ELP. * represents $p < 0.05$.

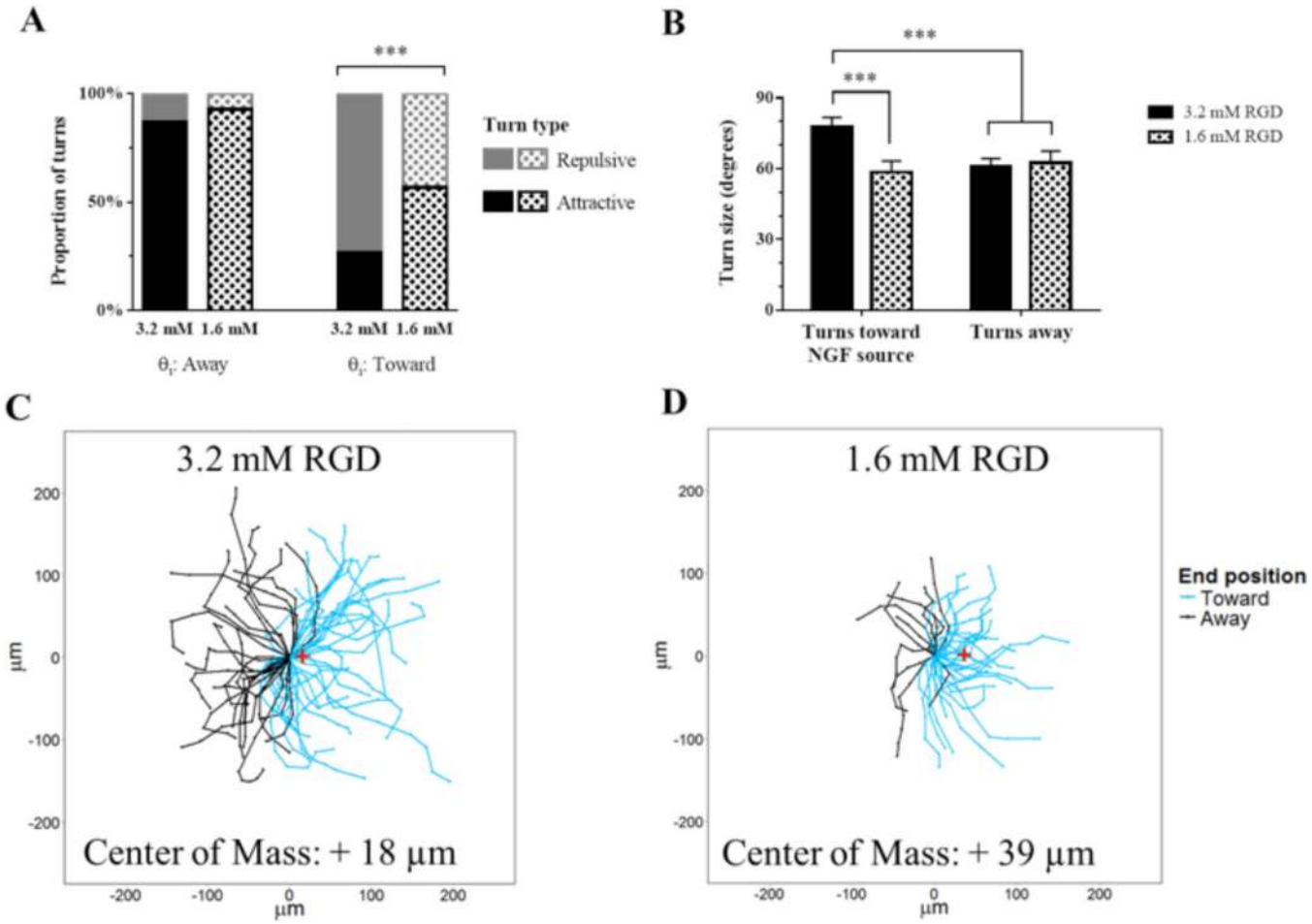

Figure 5.

Effect of RGD ligand density on neurite turning in 3D ELP matrices. **A,** Contingency analysis of neurite orientation before turning and subsequent turn direction. **B,** Turns toward the source in 3.2 mM RGD-ELP are larger on average. **C** and **D** show paths of turning neurites in 3.2 mM and 1.6 mM RGD-ELP, respectively. Neurites that make progress toward the NGF source (oriented to the right) are colored blue. The centers of mass (+) are indicated. *** represents $p < 0.005$.